

E4 ligase–specific ubiquitination hubs coordinate DNA double-strand-break repair and apoptosis

Article

Accepted Version

Ackermann, L., Schell, M., Pokrzywa, W., Kevei, E. ORCID: <https://orcid.org/0000-0002-0560-9208>, Gartner, A., Schumacher, B. and Hoppe, T. (2016) E4 ligase–specific ubiquitination hubs coordinate DNA double-strand-break repair and apoptosis. *Nature structural & molecular biology*, 23 (11). pp. 995-1002. ISSN 1545-9985 doi: 10.1038/nsmb.3296 Available at <https://centaur.reading.ac.uk/67193/>

It is advisable to refer to the publisher's version if you intend to cite from the work. See [Guidance on citing](#).

To link to this article DOI: <http://dx.doi.org/10.1038/nsmb.3296>

Publisher: Nature Publishing Group

All outputs in CentAUR are protected by Intellectual Property Rights law, including copyright law. Copyright and IPR is retained by the creators or other copyright holders. Terms and conditions for use of this material are defined in the [End User Agreement](#).

www.reading.ac.uk/centaur

CentAUR

Central Archive at the University of Reading

Reading's research outputs online

**E4 LIGASE SPECIFIC UBIQUITYLATION HUBS
COORDINATE DNA DOUBLE STRAND BREAK REPAIR
AND APOPTOSIS**

**Leena Ackermann^{1,5}, Michael Schell^{1,5}, Wojciech Pokrzywa¹, Éva Kevei¹, Anton
Gartner², Björn Schumacher^{3,4,*} & Thorsten Hoppe^{1,*}**

¹Institute for Genetics and CECAD Research Center
University of Cologne
Cologne, Germany

²Centre for Gene Regulation and Expression
School of Life Sciences
University of Dundee
Scotland

³Institute for Genome Stability in Aging and Disease
Medical Faculty
University of Cologne
Cologne, Germany

⁴CECAD Research Center and Center for Molecular Medicine Cologne
University of Cologne
Cologne, Germany

⁵These authors contributed equally to this work

*Correspondence should be addressed to B.S. or T.H.

*Correspondence: bjoern.schumacher@uni-koeln.de

Phone: +49 221 478 84202

Fax: +49 221 478 84204

thorsten.hoppe@uni-koeln.de

Phone: +49 221 478 84218

Fax: +49 221 478 84217

37 Multiple protein ubiquitylation events at DNA double strand breaks (DSBs) regulate
38 damage recognition, signaling and repair. It has remained poorly understood how the
39 repair process of DSBs is coordinated with the apoptotic response. Here, we identified
40 the E4 ubiquitin ligase UFD-2 as a mediator of DNA damage-induced apoptosis in a
41 genetic screen in *Caenorhabditis elegans*. We demonstrate that upon initiation of
42 homologous recombination by RAD-51, UFD-2 forms foci that contain substrate
43 processivity factors including the ubiquitin-selective segregase CDC-48(p97), the
44 deubiquitylation enzyme ATX-3(Ataxin-3), and the proteasome. In the absence of UFD-
45 2, RAD-51 foci persist and DNA damage-induced apoptosis is prevented. In contrast,
46 UFD-2 foci are retained until recombination intermediates are removed by the Holliday
47 junction processing enzymes GEN-1, MUS-81 or XPF-1. UFD-2 foci formation also
48 requires pro-apoptotic CEP-1(p53) signaling. Our findings establish a central role for
49 UFD-2 in the coordination between the DNA repair process and the apoptotic response.

50

51 INTRODUCTION

52 DNA double strand breaks (DSBs) are highly cytotoxic and require the assembly of DNA
53 damage signaling complexes and the DSB repair machinery at the DNA breaks ¹. In the *C.*
54 *elegans* germline DSBs are mainly repaired by homologous recombination (HR) ². After
55 initial processing of the damaged site, RAD-51 accumulates on single stranded DNA
56 (ssDNA) overhangs and mediates strand invasion into the undamaged template, thus
57 facilitating recombination and repair. Ultimately cruciform recombination intermediates
58 called Holliday junctions (HJ) are formed ³. HJs can be processed by two major pathways: HJ
59 dissolution via the combined action of the Bloom's syndrome helicase and Topoisomerase
60 TopoIIIα ⁴, or by resolution of HJs by nucleases acting as resolving enzymes ⁵. While HJ
61 dissolution predominates in most systems ^{6,7}, in *C. elegans* the GEN-1 resolvase is needed for

62 completion of HR repair of DSBs⁸. The resolution of HR intermediates is important for the
63 apoptotic response to DSBs as GEN-1 and HJ processing factors are required for DNA
64 damage-induced programmed cell death. While the mechanisms for such regulation are not
65 known yet, the C-terminal non-catalytic domain of GEN-1 appears to be important for DNA
66 damage signaling^{8,9}. The apoptotic response to persistent DSBs facilitates the removal of
67 germ cells in *C. elegans* when DSBs or meiotic recombination intermediates are not repaired,
68 and occurs in the meiotic pachytene zone of the nematode germline¹⁰. DNA damage
69 checkpoint signaling leads to the activation of the *C. elegans* p53 homolog CEP-1 followed
70 by the induction of apoptosis^{11,12}. CEP-1/p53 protein becomes available in the late pachytene
71 region of the germline, leading to apoptosis competency of these germ cells. CEP-1
72 expression in earlier stages of meiosis is translationally repressed by the conserved mRNA
73 binding protein GLD-1¹³. Thus, apoptosis is only initiated when aberrant meiotic
74 recombination intermediates or ionizing radiation (IR)-induced DSBs persist in late pachytene
75 cells. It remains, however, unclear how DNA damage processing by recombination repair is
76 coordinated with the apoptosis pathway to allow sufficient time to resolve HR intermediates.

77 In order to better understand how the apoptotic response to DSBs is regulated, we undertook a
78 genetic screen in *C. elegans* for defects in the IR-induced germ cell apoptosis. RNAi
79 knockdown and genetic mutation of *ufd-2* resulted in a reduced apoptotic response. We
80 demonstrate that upon initiation of HR by the recombinase RAD-51, UFD-2 forms foci that
81 we define as ubiquitylation hubs as they also contain substrate CDC-48, ATX-3, and the
82 proteasome. In the absence of UFD-2 or its catalytic activity, RAD-51 foci persist. Similarly
83 to *ufd-2* deficiency, elevated RAD-51 levels result in reduced apoptosis. When the resolution
84 of HJs is hampered due to the absence of GEN-1, MUS-81, or XPF-1, UFD-2 foci persist.
85 UFD-2 foci formation not only requires RAD-51 but also pro-apoptotic signaling through the
86 *C. elegans* p53 homolog CEP-1. We thus propose that UFD-2 specific ubiquitylation hubs

87 link pro-apoptotic and DNA repair signaling to coordinate the apoptotic response with
88 ongoing DSB repair activity.

89

90 **RESULTS**

91 **Ligase activity of UFD-2 triggers DSB-induced apoptosis**

92 To identify new regulators of the apoptotic response to DNA damage, we performed an RNA
93 interference (RNAi) screen targeting 770 genes whose transcription is enriched in the *C.*
94 *elegans* germline¹⁴ (**Fig. 1a**). We focused on those candidate genes because in *C. elegans*
95 DNA damage induced apoptosis only occurs in germ cells^{10,15}. We identified the E4 ubiquitin
96 ligase UFD-2 as the most prominent hit resulting from our screen. RNAi against *ufd-2* led to a
97 dose dependent reduction of IR induced apoptosis (**Fig. 1b**), a phenotype confirmed by
98 analyzing the two different null alleles *ufd-2(tm1380)* and *ufd-2(hh1)* (**Fig. 1c, d**). In contrast,
99 neither developmental apoptosis that occurs during the somatic development of the worm, nor
100 physiological germ cell apoptosis, a background level of germ cell apoptosis that occurs
101 independently of DNA damage, was defective in *ufd-2* mutants (**Supplementary Fig. 1a, b**).

102 UFD-2 participates in the ubiquitin fusion degradation (UFD) pathway that was first
103 identified in budding yeast¹⁶. Substrate ubiquitylation involves E1 ubiquitin activating, E2
104 ubiquitin conjugating, and E3 ubiquitin ligase enzymes. UFD-2 defines a class of so-called E4
105 enzymes, which further elongate pre-existing ubiquitin chains to facilitate efficient
106 proteasomal degradation¹⁷⁻²⁰. It preferentially targets lysine residues 29 and 48 of ubiquitin
107 for autoubiquitylation (**Supplementary Fig. 1e**). A P951A point mutation in the U-box
108 domain completely blocks the ligase activity of UFD-2²¹ (**Fig. 1e**). To determine if UFD-2
109 catalytic activity was required for DNA damage-induced apoptosis, we transgenically
110 expressed UFD-2::GFP or UFD-2^{P951A}::GFP in the germline of wild-type or the *ufd-2* deletion

background. Importantly, UFD-2::GFP expression fully restored the apoptotic DNA damage response in *ufd-2(tm1380)* mutant animals (**Fig. 1f**). In contrast, the catalytically dead mutant UFD-2^{P951A}::GFP showed strongly reduced apoptosis after treatment with 60 Gy IR comparable to *ufd-2* deletion mutant. Overexpression of UFD-2^{P951A}::GFP in the wild-type background also caused defective apoptosis, which indicates that the inactive U-box mutant acts dominant-negatively in response to DNA damage (**Fig. 1f**).

UFD-2 forms focal accumulations upon DSB induction

To determine *in vivo* localization, we raised polyclonal antibodies that specifically recognize UFD-2 both by western blot analysis and immunofluorescence staining (**Fig. 2a and Supplementary Fig. 2a**). Using immunostaining, we found that under unperturbed conditions the protein was evenly distributed in the *C. elegans* germ line syncytium (**Supplementary Fig. 2b**). Commencing from late pachytene cells, UFD-2 accumulated at the nuclear periphery resulting in a ring-shaped staining pattern. After IR treatment, UFD-2 foci of varying size and number became detectable within the nucleoli (**Fig. 2a, b and Supplementary Fig. 2b**). The pattern of antibody staining was confirmed by GFP-tagged UFD-2 transgenes (**Fig. 2c, d**). These UFD-2 foci occurred in the mitotic zone (data not shown) as well as in the mid-late pachytene zone of the germline after IR (**Supplementary Fig. 2b**). Given our interest in apoptosis we focused on UFD-2 foci formation in the pachytene region. Pachytene cells elicit DNA damage-induced apoptosis upon DNA damage checkpoint activation, whereas mitotic nuclei in the distal germ line compartment are subjected to cell cycle arrest¹⁰. In contrast to the IR-induced apoptosis defect, the cell cycle arrest, which can be monitored by scoring the number of mitotic nuclei that are enlarged due to continuous growth of cellular and nuclear compartments in the absence of cell division (**Supplementary Fig. 1c, d**)^{10,22}, was normally induced in *ufd-2* mutant animals, suggesting that the DNA damage checkpoint in general was

functional. Unlike IR-induced RAD-51 repair foci, which accumulate immediately upon damage induction, UFD-2 foci were not yet detectable 5 hrs following damage (**Supplementary Fig. 2c, d**). We therefore scored UFD-2 foci formation 24 hrs after IR, a time concurrent with full apoptosis activation¹⁰, using both antibodies and GFP transgenes. The number of foci observed in pachytene cells increased from 0-5 foci per germline to more than 15 upon treatment with 60 Gy of IR (**Fig. 2a-d and Supplementary Fig. 2b, c**). Surprisingly, the ubiquitin ligase mutant was equally efficient in UFD-2 foci formation as the wild-type ligase (**Fig. 2 c, d**). Together, these data indicate that the UFD-2 ligase activity is required to trigger DNA damage-induced apoptosis (**Fig. 1f**), but is not necessary for UFD-2 foci formation (**Fig. 2c, d**).

Ubiquitin signaling fine-tunes the apoptotic response

Given that UFD-2 triggers protein degradation^{16,17,23}, we examined if factors associated with the ubiquitin-proteasome system (UPS) might associate with UFD-2 foci^{17,24,25}. Hence, we analyzed ubiquitin localization 24 hrs after irradiation. In fact, an antibody recognizing conjugated mono- and polyubiquitin chains co-stained UFD-2 foci (**Fig. 3a and Supplementary Fig. 3e**). Additional staining experiments detected co-localization of the proteasome and the ubiquitin-selective segregase CDC-48 with UFD-2 foci (**Fig. 3a**). Among other processes, CDC-48/p97 has been established to coordinate the degradation of chromatin-associated proteins during DNA replication or DNA repair by extracting ubiquitylated substrate proteins from higher order complexes²⁶⁻²⁸. As CDC-48 has been shown to interact with UFD-2²⁰, we wondered if the interaction was necessary for UFD-2 dependent apoptotic signaling. Transgenic overexpression of UFD-2^{C448Y}::GFP, a mutant version that provides ligase activity but is not able to interact with CDC-48²⁹, led to UFD-2 foci even without IR treatment (**Supplementary Fig. 3f-j**). However, UFD-2^{C448Y}::GFP failed

to rescue the apoptosis phenotype displayed by *ufd-2* deletion worms (**Fig. 3g**), suggesting that in addition to ligase activity also the interaction with CDC-48 is a prerequisite for the apoptotic function of UFD-2. CDC-48 has been demonstrated to guide ubiquitin chain topology by coordinating different substrate processing enzymes such as UFD-2 and the deubiquitylation enzyme ATX-3²⁰. Intriguingly, we also found that ATX-3 localized to UFD-2 foci (**Fig. 3a and Supplementary Fig. 3c, d**), which indicates an orchestrated action of UFD-2, ATX-3, and CDC-48 at ubiquitylation hubs triggered by DNA damage. The ubiquitylation activity of UFD-2 was dispensable for the recruitment of the proteasome, ATX-3, and CDC-48 (**Fig. 3b**). In contrast, apoptosis induction required the catalytic activity of UFD-2 as well as its interaction with CDC-48 (**Fig. 1e, f, and 3g**).

Given that in yeast and humans, Ufd2/UBE4B mediates elongation of preformed ubiquitin chains, we tested whether UFD-2 cooperates with the E3 ligase HECD-1, the ortholog of budding yeast Ufd4 and human HECTD1 or TRIP12, to trigger DNA damage induced apoptosis^{17,30-32}. Indeed, loss of HECD-1 prevented UFD-2 foci formation, suggesting ubiquitin-dependent recruitment of UFD-2 (**Fig. 3c, d**). Apoptosis was reduced in *hecd-1* mutants, which implicates a role of UFD-2 focal accumulation in response to DNA damage (**Fig. 3e**). The apoptosis defect was even more pronounced in *ufd-2; hecd-1* double mutants, indicating that the activity of both enzymes is required to achieve apoptosis (**Fig. 3e**). In contrast, the deubiquitylation enzyme ATX-3 counteracted UFD-2 recruitment as both UFD-2 foci formation and apoptosis were increased in *atx-3* mutants (**Fig. 3c, d, f**). Accordingly, the excessive DNA damage-induced apoptosis occurring in *atx-3* mutants was suppressed in *ufd-2; atx-3* double mutant worms (**Fig. 3f**). The number of ubiquitin foci per germline was decreased in *hecd-1*, whereas it was increased in *atx-3* (**Fig. 3c, d and Supplementary Fig. 3k**). This observation suggests ubiquitin dependent formation of UFD-2 foci, determined by ubiquitin-mediated recruitment signals fine-tuned by HECD-1 and ATX-

3. We therefore conclude that the apoptotic response to DNA damage is coordinated by ubiquitylation signals defined by UFD-2 in cooperation with HECD-1 and ATX-3.

UFD-2 supports RAD-51 dissociation from DNA repair sites

Next we analyzed if UFD-2 also affects the DNA repair process in addition to apoptosis. In contrast to DSB induction by IR, UV irradiation did not result in formation of UFD-2 foci consistent with a specific role of UFD-2 in responding to DSBs (**Supplementary Fig. 3a**). In line with this observation, we found that RPA-1::GFP and BRD-1::GFP HR fusion proteins^{33,34} accumulate in UFD-2 foci 24 hrs after IR treatment (**Fig. 4a, b**). Furthermore, IR of L4 staged *ufd-2* mutant larvae resulted in reduced embryonic survival in the ensuing generation (**Supplementary Fig. 3b**). To establish whether *ufd-2* promotes the processing of DNA repair intermediates, we analyzed the kinetics of RAD-51 foci. While both wild-type and *ufd-2* mutants accumulated an equal amount of RAD-51 positive nuclei one hour after IR, twice as many RAD-51 stained nuclei persisted 16 hrs later in *ufd-2* mutants (**Fig. 4c, d**). This delay in RAD-51 foci dissociation that temporally coincides with UFD-2 foci formation suggests that UFD-2 contributes to resolution of repair intermediates.

UFD-2 acts downstream of pro-apoptotic signaling

We next wished to further investigate the role of the DSB repair process in UFD-2 foci formation (**Fig. 4a**). Impairment of HR in *rad-51* deletion mutant worms blocked UFD-2 foci formation (**Fig. 5b**). Conversely, *rad-54* deletion defective in removal of RAD-51 from DNA during HR repair³⁵ caused an accumulation of UFD-2 foci (**Fig. 5b**). The nucleases GEN-1, MUS-81 and XPF-1 are required for the resolution of HJs in order to complete the HR repair process of IR-induced DSBs^{8,36,37}. Deletion of the *gen-1*, *mus-81*, and/or *xpf-1* HJ processing enzymes also led to focal accumulation of UFD-2 (**Fig. 5c and Supplementary Fig. 4a**). Of

note, *mus-81* and *xpf-1* mutant animals showed elevated numbers of UFD-2 foci also in the absence of IR-induced DSBs consistent with the function of MUS-81/XPF-1 in meiotic HJ resolution^{36,37}. These results indicate that HR needs to commence for UFD-2 foci to form, which persist until HR is completed (**Fig. 5b, c**).

As *ufd-2* mutant worms displayed reduced apoptosis, we assessed whether apoptotic signaling was affected in *ufd-2* mutant worms. The apoptotic core machinery is conserved from *C. elegans* to the mammalian system. The p53 homologue CEP-1 induces transcription of the two BH3-only proteins EGL-1 and CED-13^{13,38}, which bind to the only Bcl2-like protein CED-9. As a consequence, the inhibitory effect of CED-9 on the Apaf1-like CED-4 is alleviated and CED-4 activates the caspase CED-3, which executes cell death (**Fig. 5a**)³⁹. In view of the ubiquitin ligase activity, we tested whether CEP-1 protein might accumulate upon DNA damage in the absence of UFD-2. However, in wild-type and *ufd-2* mutant worms CEP-1 protein was equally expressed following 60 Gy irradiation (**Supplementary Fig. 4b-d**). Additional evaluation of mRNA transcripts of the CEP-1 target gene *egl-1* showed a comparable transcriptional regulation in both genotypes 4 and 24 hrs after damage infliction (**Supplementary Fig. 4d**). Having established that CEP-1 activation occurs independently of *ufd-2*, we wondered if UFD-2 foci formation might be dependent on CEP-1. Strikingly, loss of CEP-1 prevented UFD-2 foci induction after IR (**Fig. 5d**), whereas UFD-2 protein expression remained unaffected (**Supplementary Fig. 5b**). Consistently, a double mutant of the two pro-apoptotic CEP-1 effectors, *egl-1; ced-13*, which is similarly defective in DNA damage-induced apoptosis as *cep-1* mutants⁴⁰, phenocopied the *cep-1* defect in UFD-2 foci formation after DNA damage (**Fig. 5d and Supplementary Fig. 5a**). To further confirm a direct role of CEP-1 in UFD-2 foci formation, we enhanced CEP-1 activity by employing a *gld-1(op236)* mutation, previously shown to increase CEP-1 levels¹³. *gld-1* mutants indeed displayed strongly elevated UFD-2 foci, supporting the idea that CEP-1 promotes UFD-2

focal accumulation. The *cep-1*; *gld-1* double mutant displayed a similar number of UFD-2 foci as wild-type germ cells (**Fig. 5d and Supplementary Fig. 5a**). One potential explanation for the failure of *cep-1* to completely suppress the foci formation in *gld-1* might be the numerous additional target mRNAs of GLD-1^{41,42}. Of note, the failure of *cep-1* to initiate apoptosis does not affect repair activity as IR-induced embryonic lethality has previously been shown to remain unaffected¹³. Consistently, we found that RAD-51 foci disassembly 16 hrs after damage induction was as efficient in *cep-1* and *gld-1* mutants as in wild-type (**Supplementary Fig. 5c**). In contrast to the loss of CEP-1 signaling, UFD-2 foci formation was unaltered in apoptosis deficient *ced-3* and *ced-4* mutant worms (**Fig. 5d**), emphasizing the necessity of CEP-1 activity for UFD-2 foci formation rather than the apoptotic process in general. Taken together, UFD-2 seems to act downstream of the pro-apoptotic signaling cascade.

Resolution of RAD-51 is linked to apoptotic signaling

We next wished to investigate the role of UFD-2 in the removal of RAD-51 foci and its consequence on apoptosis. Germline-specific expression of UFD-2::GFP in transgenic *ufd-2* deletion mutants rescued the delay of RAD-51 removal from DNA (**Fig. 6a**). Increased RAD-51 retention occurred in moderately RAD-51::GFP overexpressing worms after 24 hrs of IR compared to wild-type (**Fig. 6a**). Importantly, the retention of RAD-51 filaments either by loss of *ufd-2* or by RAD-51 overexpression strictly correlated with reduced apoptosis levels (**Fig. 6b**). Despite the elevated RAD-51 protein levels, the GFP transgenic line possessed normal repair capacity as assessed by embryonic survival after IR thus suggesting that the reduced apoptosis is not related to enhanced removal of DSBs (**Supplementary Fig. 6a**). Conversely, the *atx-3* mutant, which displayed increased UFD-2 foci and apoptosis after DNA damage, showed decreased RAD-51 retention 16 hrs after IR (**Supplementary Fig. 6b**). To

test whether elevated RAD-51 levels might directly account for the reduced apoptosis observed in *ufd-2* mutants or upon overexpression of RAD-51, we depleted RAD-51 by RNAi knockdown. Indeed, *rad-51*(RNAi) in *ufd-2* mutant or RAD-51::GFP expressing worms reverted the apoptosis defect following IR treatment (**Fig. 6c**). Importantly, *rad-51*(RNAi) also reduced embryonic survival after IR in wild-type and *rad-51* mutant worms (**Supplementary Fig. 6c**). We further validated the role of RAD-51 filaments in suppressing the apoptotic response by inhibition of RAD-51 filament formation with the RAD-51 inhibitor B02⁴³. Similarly to reduced RAD-51 levels, treatment with B02 reverted the apoptosis phenotype of *ufd-2* deletion mutants or the RAD-51 overexpression line (**Fig. 6d**), suggesting that RAD-51 accumulation directly antagonizes apoptotic signaling. Moreover, *rad-51* heterozygous mutants with reduced RAD-51 levels reverted the apoptosis defect of *ufd-2* mutants (**Fig. 6e**). In summary, these observations support the idea that UFD-2 contributes to resolution of DNA repair sites and that retention of RAD-51 filaments leads to inhibition of apoptosis (**Fig. 6f**).

DISCUSSION

In this study we uncovered a ubiquitin dependent process that facilitates the communication between DNA repair and the apoptotic response. We implicated the E4 ubiquitin ligase UFD-2 as a central regulator for the spatiotemporal coordination of both processes. Our data suggest that defects in timely proceeding of HR either by failure to resolve HJs as previously demonstrated^{8,9} or by aberrant retention of RAD-51 foci at the chromatin caused by loss of UFD-2 as shown here, halt the apoptotic response. Conversely, RAD-51 filament assembly and pro-apoptotic signaling by the p53 tumor suppressor homolog CEP-1 are both required for the formation of UFD-2-specific hubs that we define by the presence of proteolytic factors of the UPS machinery (**Fig. 6f**). We propose that these degradation hubs calibrate the proceeding of the DNA repair machinery with apoptotic activity via modulation of ubiquitin

signaling. Such a calibration might allow gaining time for ongoing HR repair when CEP-1 dependent apoptotic signaling has already been triggered. Indeed, CEP-1 activity can be detected within the first hour following IR treatment⁴⁰, while the rapidly formed RAD-51 foci are turned over in the course of 24 hrs. To prevent the precocious demise of cells that are engaged in the process of repairing DSBs, the simultaneous presence of pro-apoptotic signaling and ongoing HR requires coordination, which we propose is orchestrated at the HR repair sites through the UFD-2-ubiquitin hubs that might thus provide feedback to the apoptotic signaling on the status of the damage removal. The fine-tuning of ubiquitin chain topology by concerted action of UFD-2, the E3 ligase HECD-1 and the hydrolase ATX-3 at HR sites might indeed constitute a versatile signaling tool to enable communication between the apoptotic response and DNA damage (**Fig. 6f**). Since the E3 ligase HECD-1 is required for UFD-2 hub formation and apoptosis execution, we propose that E4 activity^{17,31,44} is providing an additional layer of regulation by editing ubiquitin chain topology. The human E4 homolog UBE4B cooperates similarly with the HECT domain E3 ligase TRIP12 in substrate ubiquitylation, suggesting the existence of a conserved signaling pathway³⁰. In support of this idea, TRIP12 fine-tunes ubiquitin controlled events at DSBs⁴⁵ and recent reports linked UBE4B to different cancer types, highlighting the relevance of ubiquitin signaling in the decision between DNA damage and apoptosis response⁴⁶⁻⁴⁹. Disassembly of RAD-51 filaments might involve the ubiquitin-selective segregase CDC-48/p97, which was recently implicated in chromatin associated protein degradation^{26,27}. Moreover, Cdc48 was shown to limit RAD51 occupancy on DNA⁵⁰. In agreement with this notion, CDC-48 binding is required for UFD-2 to trigger DNA damage induced cell death (**Fig. 3g**). Defects in DNA repair and apoptosis are especially relevant in tumor formation. Thus, understanding the conserved role of UFD-2/UBE4B in response to IR induced DNA damage might open new therapeutic directions for drug development and cancer treatment.

Acknowledgements We thank Y. Kohara, M. Marr, the *Caenorhabditis* Genetics Center (funded by the NIH National Center for Research Resources), the Bloomington Stock Center, the Dana-Farber Cancer Institute, Addgene and Geneservice Ltd for antibodies, plasmids, cDNAs, and strains; K. Gödderz, A. Lisowski, and E. Stellbrink for technical help. We thank A. Franz and A. Gutschmidt for critical reading of the manuscript. We thank K. Ramadan and Y. Shiloh for insightful discussions on the project and exchange of unpublished results. This work was supported by a Wellcome Trust Senior Research award (090944/Z/09/Z) to A.G., grants of the German-Israeli Foundation (GIF 1104-68.11/2010), the Deutsche Forschungsgemeinschaft (EXC 229, SFB 829, SFB 670, and KFO 286), the European Research Council (ERC Starting grant 260383), Marie Curie (FP7 ITN CodeAge 316354, aDDRes 316390, MARRIAGE 316964), and the Bundesministerium für Forschung und Bildung (Sybacol FKZ0315893A-B) to B.S., and the Deutsche Forschungsgemeinschaft (EXC 229, HO 2541/8-1, and KFO 286) and the European Research Council (consolidator grant 616499) to T.H. In addition, this work was supported by COST Action (PROTEOSTASIS BM1307), supported by COST (European Cooperation in Science and Technology).

Author Contributions L.A. and M.S. designed, performed and analyzed the experiments. W.P. performed *in vitro* ubiquitylation assays. É.K. generated ATX-3 antibody. A.G. and B.S. designed and performed the RNAi screen. B.S. and T.H. supervised the design and data interpretation. L.A., B.S., and T.H. wrote the manuscript. All authors discussed the results and commented on the manuscript.

Author Information Reprints and permissions information is available at
 www.nature.com/reprints. The authors declare no competing financial interests.
 Correspondence and requests for materials should be addressed to B.S.
 (bjoern.schumacher@uni-koeln.de) or T.H. (thorsten.hoppe@uni-koeln.de).

REFERENCES

1. Hoeijmakers, J.H. Genome maintenance mechanisms for preventing cancer. *Nature* **411**, 366-374 (2001).
2. Clejan, I., Boerckel, J. & Ahmed, S. Developmental modulation of nonhomologous end joining in *Caenorhabditis elegans*. *Genetics* **173**, 1301-1317 (2006).
3. Lemmens, B.B. & Tijsterman, M. DNA double-strand break repair in *Caenorhabditis elegans*. *Chromosoma* **120**, 1-21 (2011).
4. Bizard, A.H. & Hickson, I.D. The dissolution of double Holliday junctions. *Cold Spring Harb Perspect Biol* **6**, a016477 (2014).
5. Matos, J. & West, S.C. Holliday junction resolution: regulation in space and time. *DNA Repair (Amst)* **19**, 176-81 (2014).
6. Schwartz, E.K. & Heyer, W.D. Processing of joint molecule intermediates by structure-selective endonucleases during homologous recombination in eukaryotes. *Chromosoma* **120**, 109-27 (2011).
7. West, S.C. et al. Resolution of Recombination Intermediates: Mechanisms and Regulation. *Cold Spring Harb Symp Quant Biol* (2015).
8. Bailly, A.P. et al. The *Caenorhabditis elegans* homolog of Gen1/Yen1 resolvases links DNA damage signaling to DNA double-strand break repair. *PLoS genetics* **6**(2010).
9. Silva, N., Adamo, A., Santonicola, P., Martinez-Perez, E. & Volpe, L.A. Pro-crossover factors regulate damage-dependent apoptosis in the *Caenorhabditis elegans* germ line. *Cell Death & Differentiation* **20**, 1209-1218 (2013).
10. Gartner, A., Milstein, S., Ahmed, S., Hodgkin, J. & Hengartner, M.O. A conserved checkpoint pathway mediates DNA damage--induced apoptosis and cell cycle arrest in *C. elegans*. *Molecular cell* **5**, 435-443 (2000).

- 364 11. Schumacher, B., Hofmann, K., Boulton, S. & Gartner, A. The C. elegans homolog of
365 the p53 tumor suppressor is required for DNA damage-induced apoptosis. *Current*
366 *biology : CB* **11**, 1722-1727 (2001).
- 367 12. Derry, W.B., Putzke, A.P. & Rothman, J.H. Caenorhabditis elegans p53: role in
368 apoptosis, meiosis, and stress resistance. *Science* **294**, 591-5 (2001).
- 369 13. Schumacher, B. et al. Translational repression of C. elegans p53 by GLD-1 regulates
370 DNA damage-induced apoptosis. *Cell* **120**, 357-368 (2005).
- 371 14. Reinke, V. et al. A global profile of germline gene expression in C. elegans. *Molecular*
372 *cell* **6**, 605-616 (2000).
- 373 15. Vermezovic, J., Stergiou, L., Hengartner, M.O. & d'Adda di Fagagna, F. Differential
374 regulation of DNA damage response activation between somatic and germline cells in
375 Caenorhabditis elegans. *Cell death and differentiation* **19**, 1847-1855 (2012).
- 376 16. Johnson, E.S., Ma, P.C.M., Ota, I.M. & Varshavsky, A. A Proteolytic Pathway That
377 Recognizes Ubiquitin as a Degradation Signal. *Journal of Biological Chemistry* **270**,
378 17442-17456 (1995).
- 379 17. Koegl, M. et al. A novel ubiquitination factor, E4, is involved in multiubiquitin chain
380 assembly. *Cell* **96**, 635-644 (1999).
- 381 18. Saeki, Y., Tayama, Y., Toh-e, A. & Yokosawa, H. Definitive evidence for Ufd2-
382 catalyzed elongation of the ubiquitin chain through Lys48 linkage. *Biochemical and*
383 *biophysical research communications* **320**, 840-845 (2004).
- 384 19. Hoppe, T. Multiubiquitylation by E4 enzymes: 'one size' doesn't fit all. *Trends*
385 *Biochem Sci* **30**, 183-7 (2005).
- 386 20. Kuhlbrodt, K. et al. The Machado-Joseph disease deubiquitylase ATX-3 couples
387 longevity and proteostasis. *Nat Cell Biol* **13**, 273-81 (2011).
- 388 21. Okumura, F., Hatakeyama, S., Matsumoto, M., Kamura, T. & Nakayama, K.I.
389 Functional regulation of FEZ1 by the U-box-type ubiquitin ligase E4B contributes to
390 neuritogenesis. *The Journal of biological chemistry* **279**, 53533-53543 (2004).
- 391 22. Hodgkin, J., Horvitz, H.R. & Brenner, S. Nondisjunction Mutants of the Nematode
392 CAENORHABDITIS ELEGANS. *Genetics* **91**, 67-94 (1979).
- 393 23. Janiesch, P.C. et al. The ubiquitin-selective chaperone CDC-48/p97 links myosin
394 assembly to human myopathy. *Nat Cell Biol* **9**, 379-90 (2007).
- 395 24. Rape, M. et al. Mobilization of processed, membrane-tethered SPT23 transcription
396 factor by CDC48(UFD1/NPL4), a ubiquitin-selective chaperone. *Cell* **107**, 667-77
397 (2001).

- 398 25. Richly, H. et al. A series of ubiquitin binding factors connects CDC48/p97 to substrate
399 multiubiquitylation and proteasomal targeting. *Cell* **120**, 73-84 (2005).
- 400 26. Meerang, M. et al. The ubiquitin-selective segregase VCP/p97 orchestrates the
401 response to DNA double-strand breaks. *Nat Cell Biol* **13**, 1376-82 (2011).
- 402 27. Acs, K. et al. The AAA-ATPase VCP/p97 promotes 53BP1 recruitment by removing
403 L3MBTL1 from DNA double-strand breaks. *Nat Struct Mol Biol* **18**, 1345-50 (2011).
- 404 28. Dantuma, N.P. & Hoppe, T. Growing sphere of influence: Cdc48/p97 orchestrates
405 ubiquitin-dependent extraction from chromatin. *Trends Cell Biol* **22**, 483-91 (2012).
- 406 29. Baek, G.H., Kim, I. & Rao, H. The Cdc48 ATPase modulates the interaction between
407 two proteolytic factors Ufd2 and Rad23. *Proc Natl Acad Sci U S A* **108**, 13558-63
408 (2011).
- 409 30. Park, Y., Yoon, S.K. & Yoon, J.-B.B. TRIP12 functions as an E3 ubiquitin ligase of
410 APP-BP1. *Biochemical and biophysical research communications* **374**, 294-298
411 (2008).
- 412 31. Liu, G., Rogers, J., Murphy, C.T. & Rongo, C. EGF signalling activates the ubiquitin
413 proteasome system to modulate *C. elegans* lifespan. *The EMBO journal* **30**, 2990-3003
414 (2011).
- 415 32. Shaye, D.D. & Greenwald, I. OrthoList: a compendium of *C. elegans* genes with
416 human orthologs. *PloS one* **6**(2011).
- 417 33. Marechal, A. & Zou, L. RPA-coated single-stranded DNA as a platform for post-
418 translational modifications in the DNA damage response. *Cell Res* **25**, 9-23 (2015).
- 419 34. Boulton, S.J. et al. BRCA1/BARD1 orthologs required for DNA repair in
420 *Caenorhabditis elegans*. *Curr Biol* **14**, 33-9 (2004).
- 421 35. Solinger, J.A., Kiianitsa, K. & Heyer, W.D. Rad54, a Swi2/Snf2-like recombinational
422 repair protein, disassembles Rad51:dsDNA filaments. *Mol Cell* **10**, 1175-88 (2002).
- 423 36. Agostinho, A. et al. Combinatorial regulation of meiotic holliday junction resolution
424 in *C. elegans* by HIM-6 (BLM) helicase, SLX-4, and the SLX-1, MUS-81 and XPF-1
425 nucleases. *PLoS genetics* **9**(2013).
- 426 37. O'Neil, N.J. et al. Joint molecule resolution requires the redundant activities of MUS-
427 81 and XPF-1 during *Caenorhabditis elegans* meiosis. *PLoS Genet* **9**, e1003582
428 (2013).
- 429 38. Hofmann, E.R. et al. *Caenorhabditis elegans* HUS-1 is a DNA damage checkpoint
430 protein required for genome stability and EGL-1-mediated apoptosis. *Current biology*
431 : *CB* **12**, 1908-1918 (2002).

39. Horvitz, H.R. Genetic control of programmed cell death in the nematode *Caenorhabditis elegans*. *Cancer Res* **59**, 1701s-1706s (1999).
40. Schumacher, B. et al. *C. elegans* ced-13 can promote apoptosis and is induced in response to DNA damage. *Cell Death Differ* **12**, 153-61 (2005).
41. Lee, M.H. & Schedl, T. Identification of in vivo mRNA targets of GLD-1, a maxi-KH motif containing protein required for *C. elegans* germ cell development. *Genes & development* **15**, 2408-2420 (2001).
42. Doh, J.H., Jung, Y., Reinke, V. & Lee, M.-H.H. *C. elegans* RNA-binding protein GLD-1 recognizes its multiple targets using sequence, context, and structural information to repress translation. *Worm* **2**(2013).
43. Huang, F. & Mazin, A.V. A small molecule inhibitor of human RAD51 potentiates breast cancer cell killing by therapeutic agents in mouse xenografts. *PloS one* **9**(2014).
44. Park, Y., Yoon, S.K. & Yoon, J.-B.B. The HECT domain of TRIP12 ubiquitinates substrates of the ubiquitin fusion degradation pathway. *The Journal of biological chemistry* **284**, 1540-1549 (2009).
45. Gudjonsson, T. et al. TRIP12 and UBR5 suppress spreading of chromatin ubiquitylation at damaged chromosomes. *Cell* **150**, 697-709 (2012).
46. Krona, C. et al. Screening for gene mutations in a 500 kb neuroblastoma tumor suppressor candidate region in chromosome 1p; mutation and stage-specific expression in UBE4B/UFD2. *Oncogene* **22**, 2343-51 (2003).
47. Carén, H., Holmstrand, A., Sjöberg, R.M.M. & Martinsson, T. The two human homologues of yeast UFD2 ubiquitination factor, UBE4A and UBE4B, are located in common neuroblastoma deletion regions and are subject to mutations in tumours. *European journal of cancer (Oxford, England : 1990)* **42**, 381-387 (2006).
48. Zage, P.E. et al. UBE4B levels are correlated with clinical outcomes in neuroblastoma patients and with altered neuroblastoma cell proliferation and sensitivity to epidermal growth factor receptor inhibitors. *Cancer* **119**, 915-923 (2013).
49. Kloppsteck, P., Ewens, C.A., Forster, A., Zhang, X. & Freemont, P.S. Regulation of p97 in the ubiquitin-proteasome system by the UBX protein-family. *Biochim Biophys Acta* **1823**, 125-9 (2012).
50. Bergink, S. et al. Role of Cdc48/p97 as a SUMO-targeted segregase curbing Rad51-Rad52 interaction. *Nat Cell Biol* **15**, 526-32 (2013).

FIGURE LEGENDS

Figure 1 Ubiquitin ligase activity of UFD-2 is required for apoptosis execution. **(a)** Schematic illustration of RNAi screen for identification of DNA damage-induced apoptosis mediators. After RNAi treatment worms were subjected to IR and scored for apoptotic corpses (indicated by filled arrowheads) 24 hrs later by differential interference contrast (DIC) microscopy. Representative images of 3 independent experiments. **(b)** Apoptotic corpses in worms treated with indicated RNAi constructs and exposed to different IR doses, 24 hrs after treatment. Data represent mean \pm s.e.m. of 3 independent experiments. *n* varied from 2-11 animals, see **Supplementary Table 1**. **(c)** Representative images of late pachytene cells of *C. elegans* germline 24 hrs after IR treatment (0, 60 Gy). Filled arrowheads indicate apoptotic corpses. Scale bar 5 μ m. Representative images of 3 independent experiments. **(d)** Analysis of DNA damage induced apoptosis 24 hrs after IR treatment (0, 30 or 60 Gy) of indicated genotypes. Center lines show the medians; box limits indicate the 25th and 75th percentiles as determined by R software; whiskers extend 1.5 times the interquartile range from the 25th and 75th percentiles, outliers are represented by dots. The notches are defined as $\pm 1.58 \cdot \text{IQR} / \sqrt{n}$ and represent the 95% confidence interval for each median. Non-overlapping notches give roughly 95% confidence that two medians differ. Data of 5 independent experiments. *n* varied from 69-80 animals, see **Supplementary Table 1**. **(e)** Auto-ubiquitylation of UFD-2 with UFD-2 (wild-type) or UFD-2^{P951A} as ubiquitin ligases. Representative immunoblot of 3 independent experiments. **(f)** Analysis of DNA damage induced apoptosis 24 hrs after IR treatment (0, 60 Gy) of indicated genotypes. Statistics as in **Fig. 1d**. Data of 3 independent experiments. *n* varied from 36-63 animals, see **Supplementary Table 1**.

Figure 2 UFD-2 forms foci late after IR treatment. **(a)** Representative images of worm germlines of indicated genotypes stained with α -UFD-2 antibody and DAPI 24 hrs after IR

treatment (60 Gy). Filled arrowhead indicate nuclei with UFD-2 foci. Scale bar, 5 μ m. Representative images of 3 independent experiments and (b) corresponding quantification of UFD-2 foci in pachytene region of germlines. Data show means \pm s.e.m. of 12 independent experiments. $n = 231$ animals (wt 0 Gy) and $n = 280$ animals (wt 60 Gy). (c) Representative images of worm germlines of indicated genotypes stained with GFP-booster and DAPI 24 hrs after IR treatment (60 Gy). Filled arrowheads indicate nuclei with UFD-2 foci. Scale bar, 5 μ m. Representative images of 3 independent experiments and (d) corresponding quantification of UFD-2 foci in pachytene region of germlines. Data show means \pm s.e.m. of 3 independent experiments. n varied from 34-51 animals, see **Supplementary Table 1**.

Figure 3 UPS factors accumulate in UFD-2 hubs and balance apoptotic signaling. Representative images of (a) *ufd-2(tm1380); UFD-2::GFP* and (b) *ufd-2(tm1380); UFD-2^{P951A}::GFP* immunostained with indicated antibodies 24 hrs after IR (Gy 60). The boxed area is three times magnified (3x zoom). α -alpha SU, α -Proteasome 20S alpha subunits. Scale bars, 5 μ m. Representative images of 3 independent experiments. (c) Representative images of worm germlines of indicated genotypes immunostained with α -UFD-2 antibody and DAPI 24 hrs after IR treatment (60 Gy). Filled and empty arrowhead indicated nuclei positive or negative for UFD-2 foci, respectively. Scale bar, 5 μ m Representative images of 3 independent experiments and (d) corresponding quantification of UFD-2 foci in pachytene region of germlines. Data show means \pm s.e.m. of 3 independent experiments. n varied from 36-107 animals, see **Supplementary Table 1**. (e,f,g) Analysis of DNA damage induced apoptosis 24 hrs after IR treatment (0, 60 Gy) of indicated genotypes. Statistics as in **Fig. 1d**. Data of 3 independent experiments. n varied from 39-52 animals for (e), 38-51 animals for (f) and 34-74 animals for (g), see **Supplementary Table 1**.

Figure 4 Loss of *ufd-2* delays DSB repair processing. (a) Schematic illustration of DNA DSB repair by HR in *C. elegans*. Upon DSB induction RPA binds resected single stranded DNA,

BRD-1 acts together with BRCA-1 at DSB site, RPA is exchanged for RAD-51, which mediates strand invasion, Gen-1 resolves HJ resulting in repaired DSB. Names in brackets indicate human homologues. **(b)** Representative images of *BRD-1::GFP* and *RPA-1::GFP* germlines stained with α -UFD-2 and DAPI 24 hrs after IR treatment (60 Gy). Scale bar, 5 μ m. Representative images of 3 independent experiments. **(c)** Representative images of wild-type and *ufd-2(tm1380)* germlines isolated 16 hrs after IR treatment (20 Gy), stained with α -RAD-51 and DAPI. Filled arrowheads indicate nuclei positive for RAD-51 staining. Scale bar, 10 μ m. Representative images of 3 independent experiments. **(d)** Quantification of germ cells positive for RAD-51 staining of wild-type and *ufd-2(tm1380)* worms treated with IR (0 Gy) and isolated after 1 hr or treated with IR (20 Gy) and isolated after 1, 7, 16, 48 hrs. Data show means \pm s.e.m. of 3 independent experiments. *n* varied from 35-43 animals, see **Supplementary Table 1**. The triple asterisk indicates *P* value of ≤ 0.001 in two-tailed Student's *t*-test.

Figure 5 UFD-2 foci in repair and apoptosis after DNA damage. **(a)** Schematic illustration of apoptosis pathway in *C. elegans*. Names in brackets indicate human homologues. **(b,c,d)** Quantification of UFD-2 foci in pachytene region of germlines of indicated genotypes isolated 24 hrs after irradiation (60 Gy). Data show means \pm s.e.m. of 3 independent experiments. *n* varied from 30-113 animals for **(b)**, 34-92 animals for **(c)** and 20-202 animals for **(d)**, see **Supplementary Table 1**.

Figure 6 UFD-2 coordinates communication between repair and apoptosis after DNA damage. **(a)** Quantification of germ cells positive for RAD-51 staining of indicated genotypes treated with IR (0 or 20 Gy) and isolated after 24 hrs. Data show means \pm s.e.m. of 3 independent experiments. *n* varied from 34-63 animals, see **Supplementary Table 1**. The triple asterisk indicates *P* value of ≤ 0.001 in two-tailed Student's *t*-test. **(b)** Analysis of DNA damage induced apoptosis 24 hrs after IR treatment (0, 60 Gy) of indicated genotypes.

Statistics as in **Fig. 1d**. Data of 3 independent experiments. *n-values* varied from 61-82 animals, see **Supplementary Table 1**. (c,d,e) Analysis of DNA damage induced apoptosis 24 hrs after IR treatment (0, 60 Gy) of (c) *ufd-2* and RAD-51::GFP treated with *rad-51* or control RNAi or (d) wild-type, *ufd-2*, and RAD-51::GFP worms treated with RAD51 inhibitor B02 (200 mM) or (e) indicated genotypes. Statistics as in **Fig. 1d**. Data of 3 independent experiments. *n-values* varied from 30-47 animals for (c), 28-69 animals for (d) and 29-40 animals for (e), see **Supplementary Table 1**. (f) Model for the coordination between HR and apoptotic signaling by UFD-2. DSB repair triggers RAD-51 accumulation at ssDNA to facilitate homology pairing. After efficient strand invasion RAD-51 is removed and HJ are resolved by HJ processing enzymes (GEN-1, MUS-81 and XPF-1). UFD-2 supports RAD-51 dissociation from DSB at advanced time points. Ongoing repair is reflected by the presence of UFD-2 containing hubs late after IR. These ubiquitylation hubs contain processivity factors like CDC-48 and proteasome (not shown). Interaction between UFD-2 and CDC-48 is necessary to transduce a pro-apoptotic signal. UFD-2 hub formation is fine-tuned by the E3 ligase HECD-1, the DUB ATX-3, and pro-apoptotic CEP-1/p53 signaling.

METHODS

***C. elegans* strains.** *C. elegans* strains were cultured at 20 °C on nematode growth medium (NGM) and fed with *Escherichia coli* (*E. coli*) strain OP50 according to standard procedures⁵¹. The Bristol strain N2 was used as wild-type. Mutants and transgenic animals used in this study are listed in the following: *mus-81(tm1937) I*, *rad-54&snx-3(ok615) I/hT2 [bli-4(e937) let-?(q782) qIs48] (I;III)*, *cep-1(lg12501)I*, *ced-1(e1735)I*, *gld-1(op236)I*, *ufd-2(tm1380)II*, *ufd-2(hh1)II*, *xpf-1(tm2842) II*, *gen-1(tm2940)III*, *ced-4(n1162) III*, *hecd-1(tm2371)IV*, *rad-51(ok2218) IV/nT1[qIs51](IV;V)*, *ced-3(n717) IV*, *atx-3(gk193)V*, *egl-1(n1084n3082)V*; *ced-13(tm536)X*, , *Is[rad-51::GFP::3xFLAG]*, *gla-3(op216)I*, *hus-1(op241)I*, *unc-119(ed3)III*; *gtIs[unc-119(+), Ppie-1::GFP::rpa-1::pie-1-3'UTR]*, *hhIs121[unc-119(+), Pmex-5::ufd-2::GFP::tbb-2 3'UTR]*, *hhIs135[unc-119(+), Pmex-5 (w/o ATG)::ufd-2 (w/o TAA, P951A)::(Gly)5Ala::gfp F64LS65T(w introns/stop)::tbb-2 3'UTR]*, *hhIs134[unc-119(+), Pmex-5::ufd-2 (C448Y)::GFP::tbb-2 3'UTR]*.

The transgenic lines *hhIs121*, *hhIs134*, and *hhIs135* were generated for this study. Briefly, fosmid WRM0621dE05 was used as template to obtain the genomic sequence of *ufd-2* that was cloned together with ppJA252, pJA257 into pCG150 containing the *unc-119(+)* marker for selection of transgenic worms⁵². *ufd-2* was modified by directed mutagenesis to create *ufd-2^{P951A}* or *ufd-2^{C448Y}*. The constructs were bombarded into *unc-119(ed4)III* mutants as described previously⁵³.

No statistical method was used to predetermine sample size. The experiments were not randomized and were not performed with blinding to the conditions of the experiments. All *n*-values are specified in **Supplementary Table 1** (for data in Fig. 1-6) and **Supplementary Table 2** (for data in Supplementary Fig. 1-6).

Ionizing radiation. Synchronized hermaphrodites were grown until L4 stage and irradiated with the corresponding dose (Radiation source: 120-kV X-rays (25 mA; 0.5mm Alu-filter; ISOVOLT 160 M1/10-55, GE Sensing & Inspection Technologies) or Biobeam 8000 using Cs137 as radiation source).

RNAi treatment. RNA interference was performed using the feeding method⁵⁴. Three P0 worms were placed on IPTG (isopropylthiogalactoside) and ampicillin-containing NGM-plates seeded with *E. coli* [HT115(DE3)] expressing double-stranded RNA (dsRNA) and incubated at 15°C for 72 hrs. Three single F1 worms were transferred each to a new, freshly seeded plate and allowed to lay eggs for approximately 20 hrs. F1 worms were removed and F2 worms were allowed to grow up to the L4 stage, treated with ionizing radiation and analyzed for radiation induced apoptosis. Clones in RNAi feeding vectors were provided by Marc Vidal of Dana Farber Cancer Center.

Apoptotic corpses. For physiological apoptosis analysis, synchronized L1 larvae were grown until L4 stage. Apoptotic corpses were scored 24 hrs later. For this, worms were mounted on 3% agar pads, paralyzed with 60 nM NaN₃ and analysed via DIC microscopy⁵⁵. For DNA damage induced apoptosis worms were subjected to IR at L4 stage before apoptosis was evaluated 24 hrs later. Developmental apoptosis was assessed in L1 larvae. Therefore worms were grown until day one adulthood. 100 worms were transferred to a NGM-agar plate without *E. coli* and allowed to lay eggs until they were removed after 1 hr. Freshly hatched L1 larvae were scored for apoptotic corpses⁵⁶.

UFD-2 foci. Synchronized worms were grown until L4 larvae stage and irradiated with 0 and 60 Gy. 24 hrs later, germlines were isolated and immunostained. Number of UFD-2 foci was scored in all focal planes in pachytene germ cells. One germline per worm was scored.

Protein expression and purification. cDNAs encoding *ufd-2b*, *ufd-2b*^{C448Y}, and *ufd-2b*^{P951A} were cloned into the pET-21d expression vector (Novagen) and pGex4T1 (GE Healthcare). Recombinant proteins were expressed in *E. coli* strain BL21 Codon Plus (Novagen) and purified using the ÄKTA purifier system (GE Healthcare).

Antibody production. His-tagged purified proteins (UFD-2, ATX-3²⁰) were used for immunization of rabbits and anti-sera were affinity purified using respective GST-tagged recombinant proteins (BioGenes). For validation see **Supplementary Fig. 2a** and **3d**, respectively.

Preparation of worm lysates. Synchronized L1 larvae were grown on NGM-agar plates with OP50 bacteria until they reached adulthood. Worm lysates used for SDS-PAGE were either prepared from a distinct number of worms (n=150) or by washing worms from NGM-agar plates followed by multiple washing step with M9 buffer [3 g/l KH₂PO₄, 6 g/l Na₂ HPO₄, 5 g/l NaCl, 1 mM Mg SO₄ (added after sterilization)], until bacteria were removed. The samples were heated to 95°C for 5 min and subsequently shock-frozen in liquid nitrogen. After thawing, samples were subjected to sonication (two times for 15 s, on ice; 50% power; Sonopuls UW 2200, Bandelin) and taken up in 4 x SDS sample buffer followed by centrifugation at 15,000 rpm for 10 min.

Immunotechniques. Immunostaining of isolated germlines was done according to the ‘freeze-crack’ protocol. Worms were dissected onto polylysine-coated slides (Thermo Scientific) in 60 nM NaN₃ to isolate germlines and fixed in fixation buffer (3.7 % Formaldehyde, 0.2 % Tween 20) for 10 min with subsequent shock freezing in liquid nitrogen. This was followed by incubation in 1:1 mixture of methanol and acetone at -20 °C for 10 min. Germlines were permeabilized 3 times in 1 % PBS-Triton X-100 for 20 min followed by washing in 0.1 % PBS-Tween 20 (PBS-T) for 10 min and blocking in 10 % goat

serum in 0.1 % PBS-T. A specific staining protocol was followed for GFP-expressing lines avoiding freezing. Isolated germlines were fixed with fixation buffer for 10 min in PCR tubes, directly followed by permeabilization and blocking as described above. Germlines were incubated with primary antibody overnight at 4 °C (anti-UFD-2 1:3,000, anti-CDC-48 1:12,000⁵⁷, anti-RAD-51 1:350 (14B4, #NB100-148, Novus Biologicals⁵⁸), anti-FK2-ubiquitin 1:100 (AB_612093, #04-263, Millipore, validation on manufacturer's website), anti-Proteasome 20S alpha 1+2+3+5+6+7 antibody 1:300 (MCP231, #ab22674, abcam⁵⁹), anti-ATX-3 1:700). Incubation with the fluorescently labeled secondary antibodies (#A-11037, #R37117, Life Technologies; 1:200) or GFP-booster (#GBA-488, ChromoTek; 1:400⁶⁰) was done at room temperature for 1 hr. Germlines were mounted in DAPI Fluoromount-G medium (SouthernBiotech). For western blotting, worm lysates were separated by SDS-polyacrylamide gel electrophoresis (SDS-PAGE) and transferred to nitrocellulose membranes (Whatman, Protran). Membranes were blocked in 1x Roti-Block (Roth) and incubated with the primary antibodies overnight at 4 °C in Roti-Block (Roth; anti-ATX-3 1:10,000, anti-CDC-48 1:50,000⁵⁷, anti-UFD-2 1:20,000, anti-CEP 1:15,000¹³, anti-tubulin 1:5000 (clone DM1A, Sigma-Aldrich⁶¹)). Incubation with fluorescently labeled secondary antibodies (LiCor IRDye 680, #926-32222 and #926-32223, LiCor IRDye 800, #926-32212 and #926-32213, 1:10,000) was done at room temperature, before detection of signals using the Li-Cor Odyssey scanner. Quantification of signal intensities was done using the Odyssey V4.0 software (Li-Cor). The uncropped versions of western blots that have been used to assemble the main figures are collected in **Supplementary Fig. 7**.

Immunoprecipitation *in vivo* and *in vitro*. Worm lysates were prepared as described above and the protein concentration was determined by measuring absorption at 260nm with Nanodrop 800 UV/Vis Spectrometer. 250 µl of Dynabeads (Invitrogen) were used per reaction, washed twice with conjugation buffer [100 mM sodium phosphate, 0,15 M NaCl]

and resuspended in 1 ml 5 mM crosslinking reagent BS³ (Thermo Scientific). Crosslinking was performed on rotation wheel for 30 min at room temperature. The reaction was stopped by adding 50 µl quenching buffer [1 M Tris/HCL, pH 7.5] followed by 15 min incubation at room temperature. The beads were washed three times with 0.5 x PBS before 50 µg α-UFD-2 antibody was added and incubated for 20 min under constant rotation at room temperature. After repeated washing with 0.5 x PBS, 2.5 mg of corresponding worm protein lysate was added to the beads and incubated over night at 4 °C with rotation. For *in vitro* immunoprecipitation, antigen (UFD-2) was incubated with antibody-coupled beads for 4 hrs prior to addition of the putative binding partner (CDC-48) for an additional incubation for 4 hrs. Both proteins were added in equimolar ratio (1 mM). Elution was performed as described in the manufacturer's manual.

Microscopy and image acquisition. Immunostained germlines were imaged with AxioImager.M1/Z1 microscope with Apoptome equipped with an AxioCam MRm camera (Carl Zeiss). To allow direct comparison of signal intensities, images were recorded under identical conditions. Processing of selected pictures was done in ZEN2011 and ImageJ.

***In vitro* ubiquitylation assay.** UFD-2b::His, UFD-2b^{C448Y}::GST, and UFD-2b^{P951A}::His fusion proteins were expressed in BL21-AI *E. coli* strain and lysed in buffer A [50 mM Tris pH 7.5, 250 mM NaCl, 5 mM DTT, 1% Triton X-100, 2 mM PMSF and protease inhibitor mix; Roche]. 10 µg of the aforementioned bacterial lysate was mixed with E1 (25 ng), E2 (Let-70; 400 ng), 2 µg of FLAG::ubiquitin, energy regenerating solution (Boston Biochemicals) and ubiquitin conjugation reaction Buffer (Enzo Life Sciences). Samples were incubated at 30 °C for 1.5 hrs, terminated by boiling for 5 min with SDS-sample buffer, and resolved by SDS-PAGE followed by immunoblotting using anti-UFD-2 antibodies to monitor ubiquitylation of UFD-2.

Persistence of RAD-51 foci after IR. Synchronized worms were grown until L4 larvae stage and irradiated with 0 and 20 Gy. 1 to 48 hrs later, germlines were isolated and immunostained. Z-stacks were taken of late pachytene cells of the germline. Two focal planes covering the upper and lower part of the germline were subjected to analysis by scoring each plane for RAD-51 positive cells in the last 25 nuclei of pachytene germ cells prior entering diakinesis.

RNA isolation and real-time PCR. Total RNA was isolated using TRIzol (Invitrogen) and Qiagen RNeasy kit. Briefly, worms were washed off the plates using M9 buffer [3 g/l KH₂PO₄, 6 g/l Na₂ HPO₄, 5 g/l NaCl, 1 mM Mg SO₄ (added after sterilization)] and 600 µl TRIzol, and silica beads (1 mm diameter) were added to the samples and homogenized by Precellys tissue homogeniser. Chloroform was added and samples were vortexed vigorously before phase separation through centrifugation. The aqueous phase was transferred on the Qiagen RNeasy Mini spin column and RNA was isolated according to manufacturer's instructions. cDNA was synthesized using 200 ng total RNA and the High-Capacity cDNA Reverse Transcription Kit (Applied Biosystems). Gene expression levels were determined by real time PCR using Brilliant III Ultra-Fast SYBR Green QPCR Master Mix (Agilent Technologies) and Biorad CFX96 Real-Time PCR Detection System. Relative gene expressions were normalized to *tbg-1* (F58A4.8) mRNA levels. In the experiment three biological and three technical replicate samples were analyzed. The primer sequences used in the RT-PCR reactions are the following: *tbg-1* forward:

5'-GTACACTCCACTGATCTCTGCTGACAAG-3', *tbg-1* reverse:

5'-CTCTGTACAAGAGGCAAACAGCCATG-3'⁶², *egl-1* forward:

5'-TACTCCTCGTCTCAGGACTT-3', *egl-1* reverse: 5'-CATCGAAGTCATCGCACAT-3'.

Embryonic Survival. To determine the radiation sensitivity, L4-stage hermaphrodites were irradiated with a single dose of IR as indicated. After 12 hrs, worms were transferred to fresh

plates (three worms per plate, five plates in total) and allowed to lay eggs for 5 hrs. After this period, adults were removed and 24 hrs later the number of hatched and unhatched embryos was scored (number of hatched larvae normalized to results after mock-treatment). As a control for embryonic survival, a heterozygous deletion mutant lacking *rad-51* on one chromosome was used.

B02 treatment. Synchronized L1 larvae were grown as liquid culture in S Medium with heat inactivated (3 x 5 min at 65 °C, vortexing inbetween) *E. coli* strain OP50⁶³, containing 200 mM B02.

Mitotic germ cell cycle arrest upon IR. Worms were irradiated with 0 and 60 Gy at the late L4 larval stage as described previously¹⁰. 16 hours post-irradiation, worms were mounted on 3% agar pads and paralyzed with 60 nM NaN₃ for DIC microscopy and the distal region of the germline was scored for number of nuclei in all focal planes within a defined area of 2 µm x 6 µm.

Statistical analysis. Statistical analysis was performed using Excel (Microsoft). Statistical significance was calculated with two-tailed paired Student's t-test. Box plots were generated using BoxPlotR⁶⁴. Centre lines show the medians; box limits indicate the 25th and 75th percentiles as determined by R software; whiskers extend 1.5 times the interquartile range from the 25th and 75th percentiles, outliers are represented by dots. The notches are defined as $\pm 1.58 \cdot \text{IQR} / \sqrt{n}$ and represent the 95% confidence interval for each median. Non-overlapping notches give roughly 95% confidence that two medians differ.

51. Brenner, S. The genetics of *Caenorhabditis elegans*. *Genetics* **77**, 71-94 (1974).

722 52. Zeiser, E., Frøkjær-Jensen, C., Jorgensen, E. & Ahringer, J. MosSCI and gateway
723 compatible plasmid toolkit for constitutive and inducible expression of transgenes in
724 the *C. elegans* germline. *PloS one* **6**(2011).

725 53. Praitis, V., Casey, E., Collar, D. & Austin, J. Creation of low-copy integrated
726 transgenic lines in *Caenorhabditis elegans*. *Genetics* **157**, 1217-1226 (2001).

727 54. Timmons, L. & Fire, A. Specific interference by ingested dsRNA. *Nature* **395**, 854
728 (1998).

729 55. Gumienny, T.L., Lambie, E., Hartweg, E., Horvitz, H.R. & Hengartner, M.O. Genetic
730 control of programmed cell death in the *Caenorhabditis elegans* hermaphrodite
731 germline. *Development (Cambridge, England)* **126**, 1011-1022 (1999).

732 56. Hengartner, M.O., Ellis, R.E. & Horvitz, H.R. *Caenorhabditis elegans* gene *ced-9*
733 protects cells from programmed cell death. *Nature* **356**, 494-9 (1992).

734 57. Franz, A. et al. CDC-48/p97 coordinates CDT-1 degradation with GINS chromatin
735 dissociation to ensure faithful DNA replication. *Mol Cell* **44**, 85-96 (2011).

736 58. Lans, H. et al. DNA damage leads to progressive replicative decline but extends the
737 life span of long-lived mutant animals. *Cell Death Differ* **20**, 1709-18 (2013).

738 59. Stout, G.J. et al. Insulin/IGF-1-mediated longevity is marked by reduced protein
739 metabolism. *Mol Syst Biol* **9**, 679 (2013).

740 60. Pourkarimi, E., Greiss, S. & Gartner, A. Evidence that CED-9/Bcl2 and CED-4/Apaf-
741 1 localization is not consistent with the current model for *C. elegans* apoptosis
742 induction. *Cell Death Differ* **19**, 406-15 (2012).

743 61. Gonczy, P. et al. Dissection of cell division processes in the one cell stage
744 *Caenorhabditis elegans* embryo by mutational analysis. *J Cell Biol* **144**, 927-46
745 (1999).

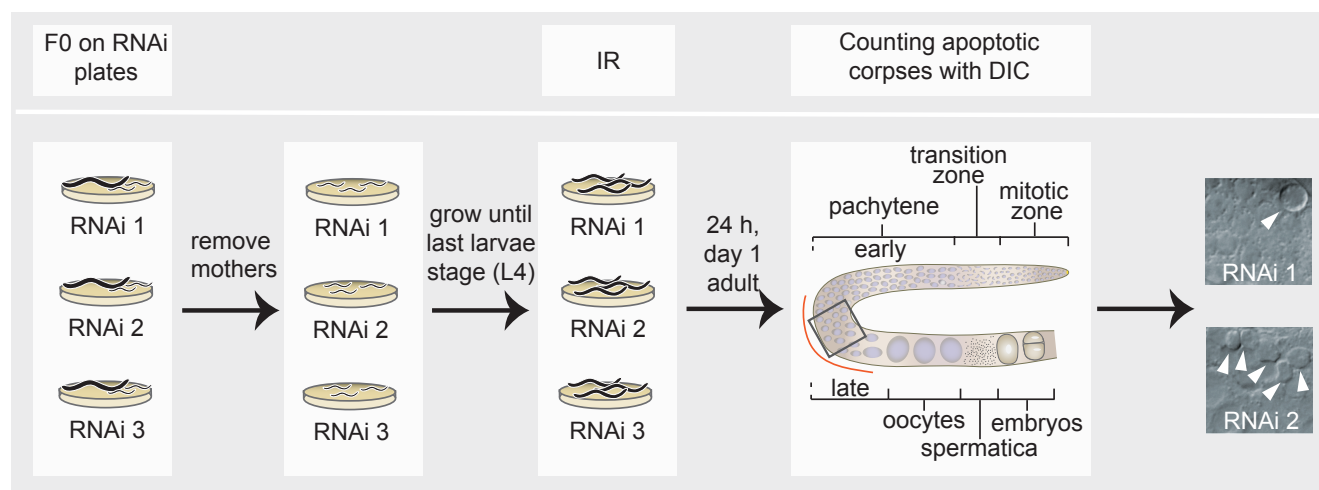
746 62. Hoogewijs, D., Houthoofd, K., Matthijssens, F., Vandesompele, J. & Vanfleteren, J.R.
747 Selection and validation of a set of reliable reference genes for quantitative sod gene
748 expression analysis in *C. elegans*. *BMC molecular biology* **9**, 9 (2008).

749 63. Lewis, J.A. & Fleming, J.T. Basic culture methods. *Methods Cell Biol* **48**, 3-29
750 (1995).

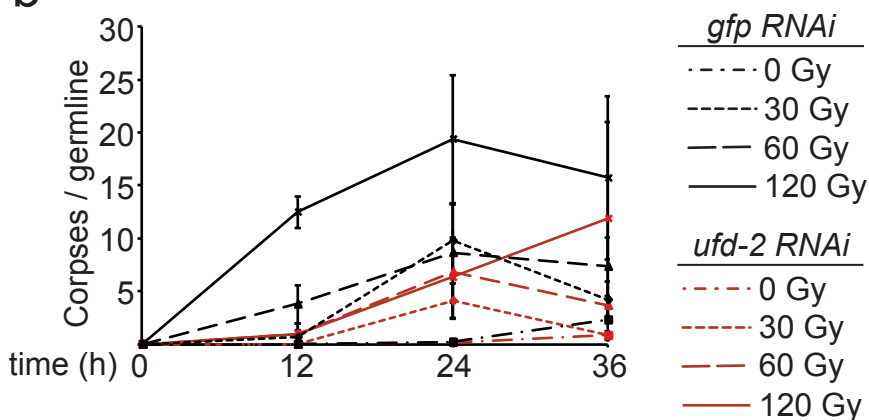
751 64. Spitzer, M., Wildenhain, J., Rappsilber, J. & Tyers, M. BoxPlotR: a web tool for
752 generation of box plots. *Nature methods* **11**, 121-122 (2014).

Figure 1

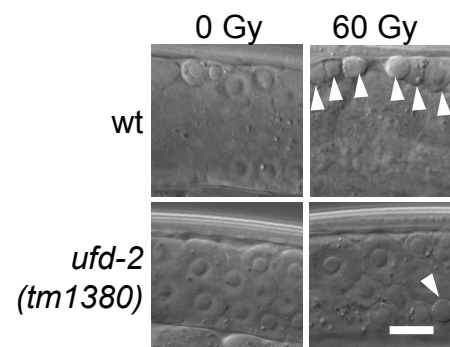
a



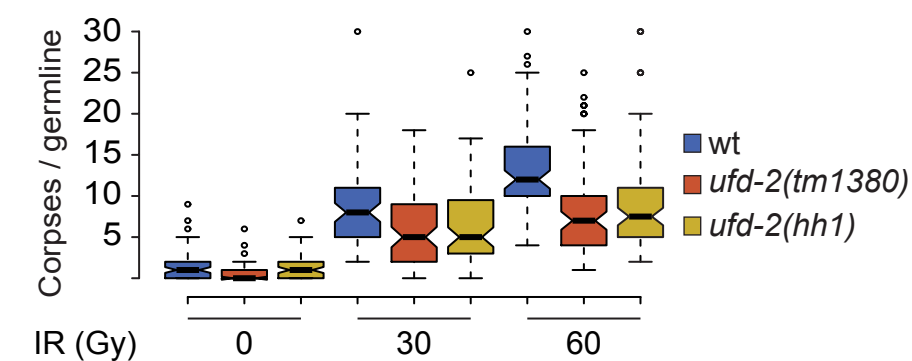
b



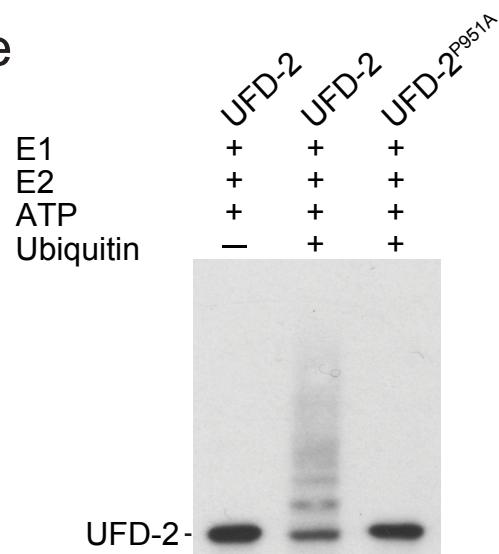
c



d



e



f

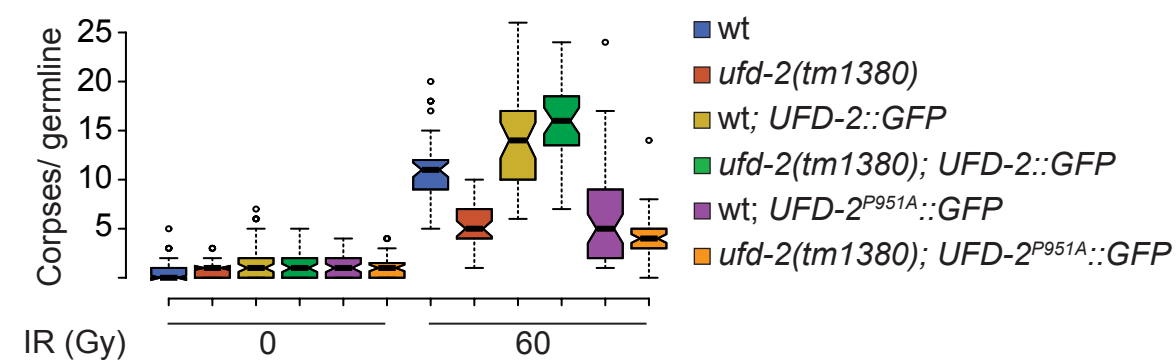
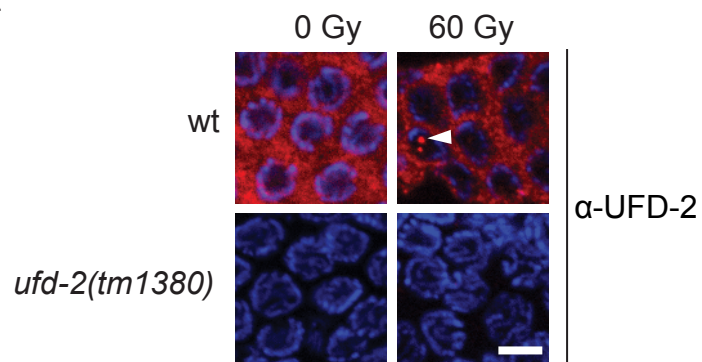
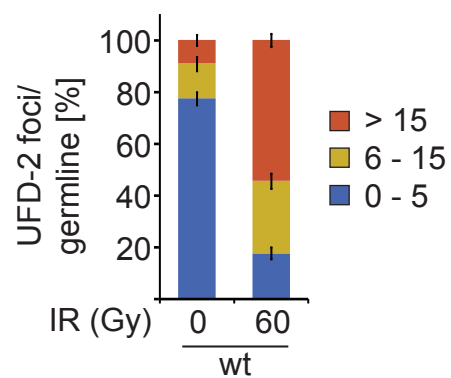


Figure 2

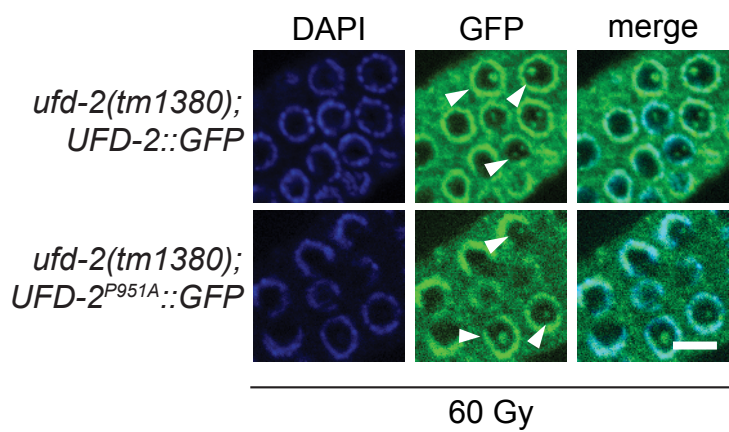
a



b



c



d

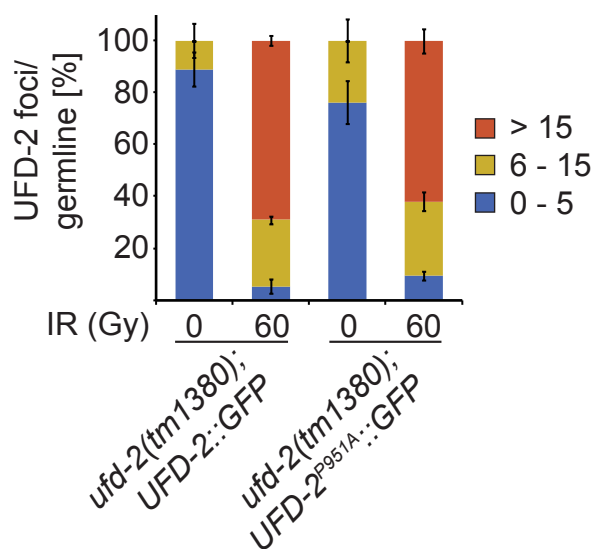
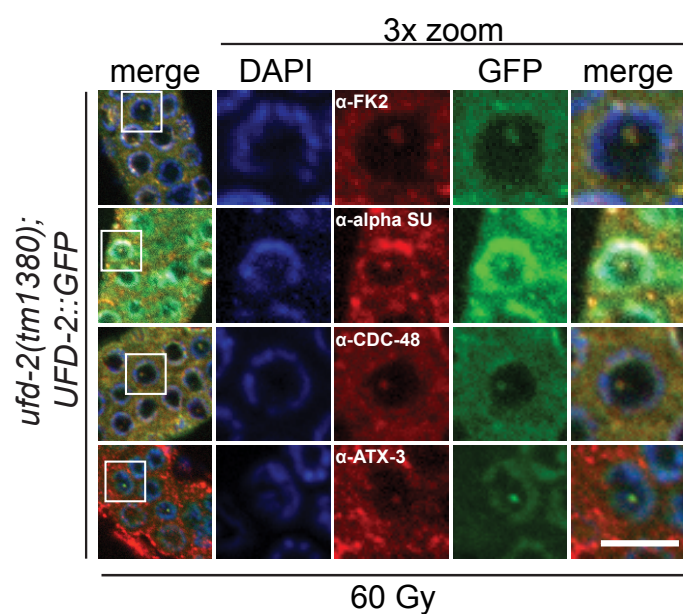
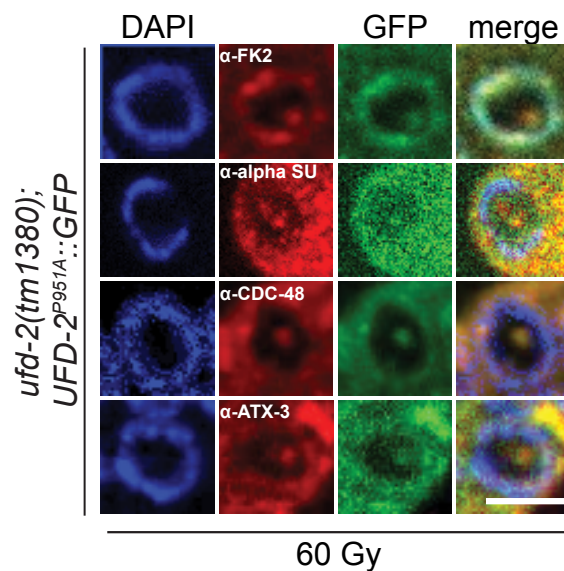


Figure 3

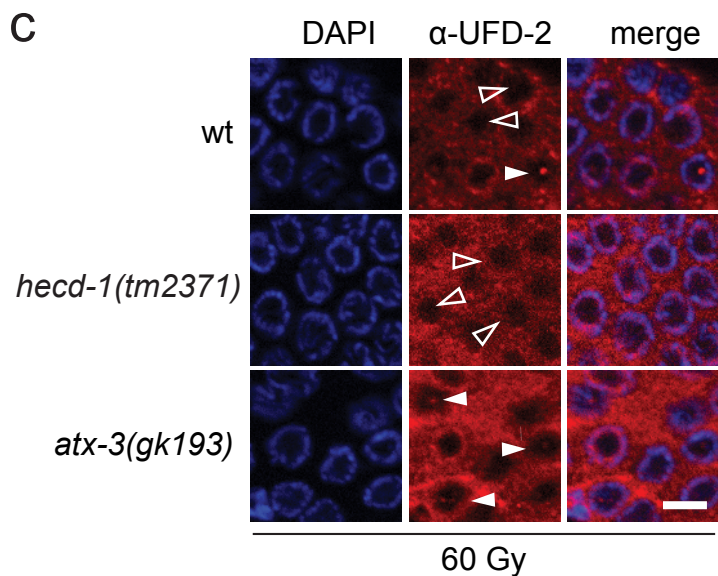
a



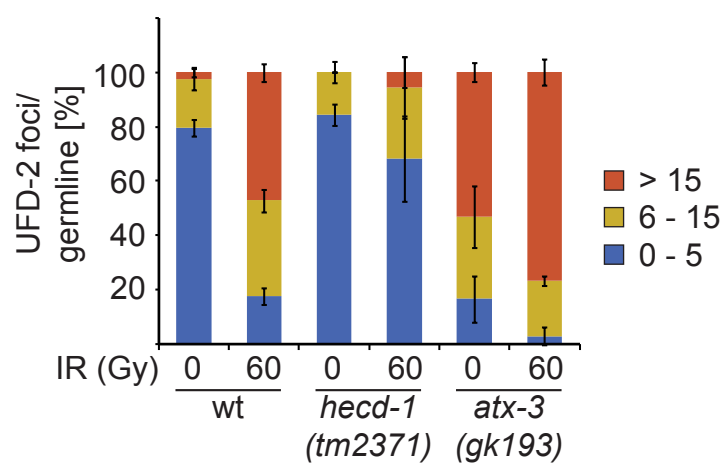
b



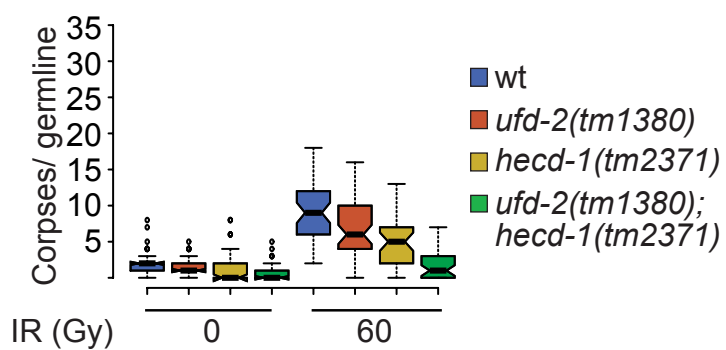
c



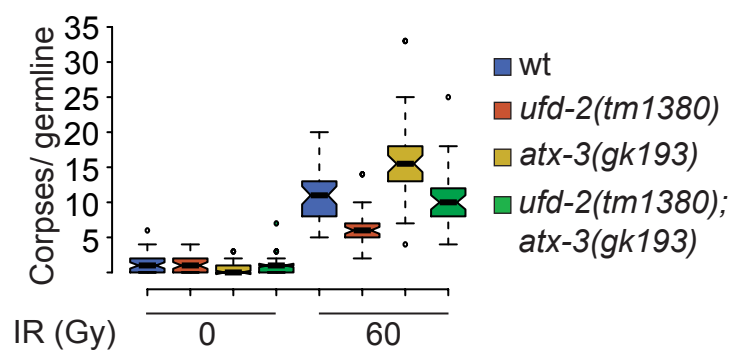
d



e



f



g

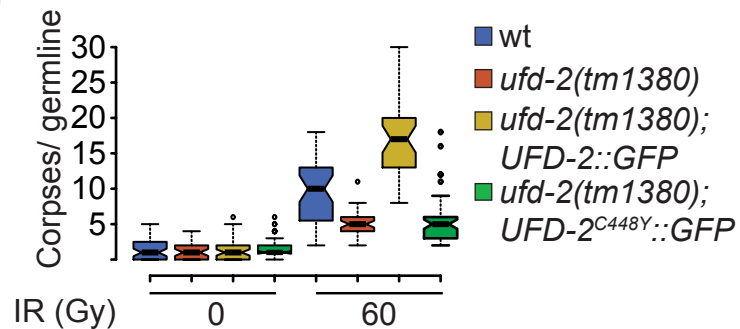
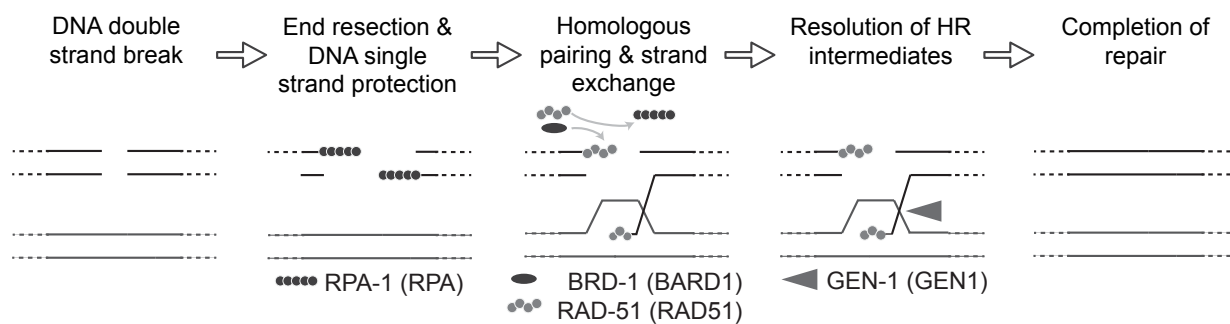
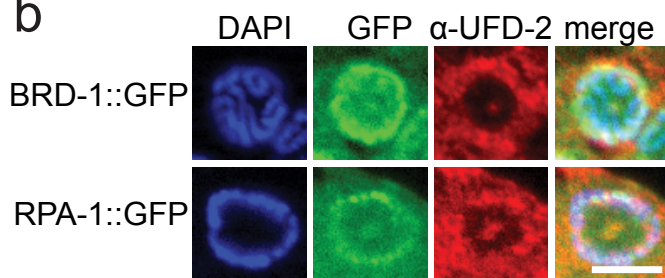


Figure 4

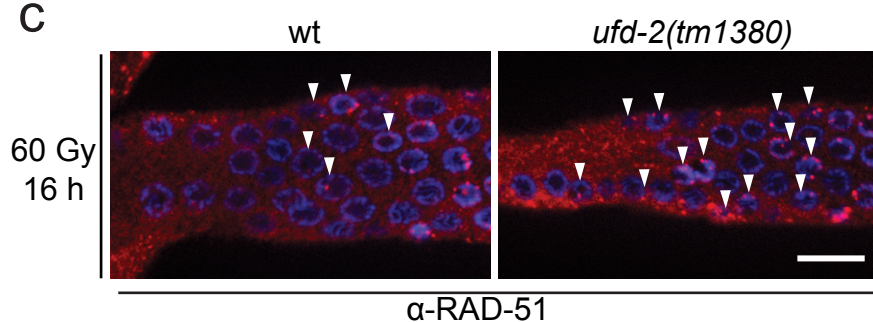
a



b



c



d

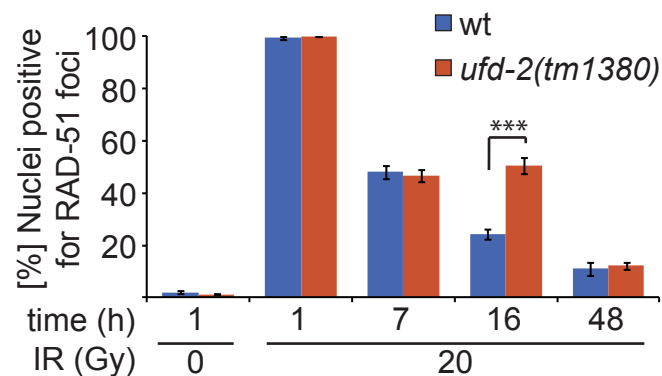


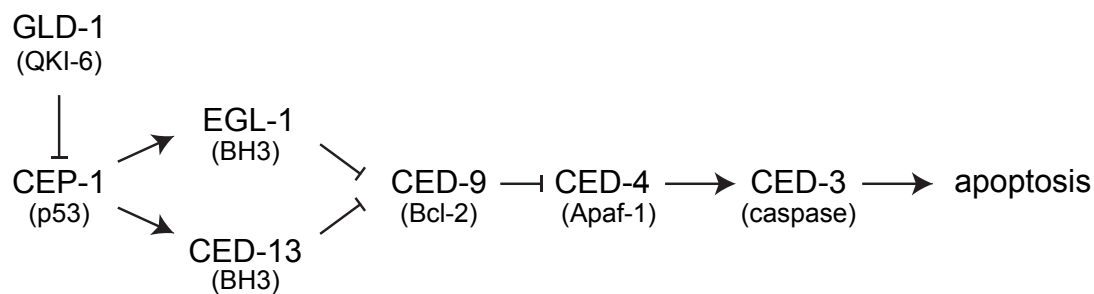
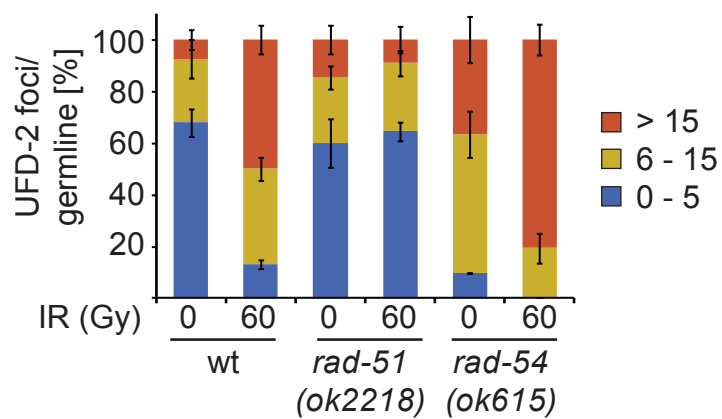
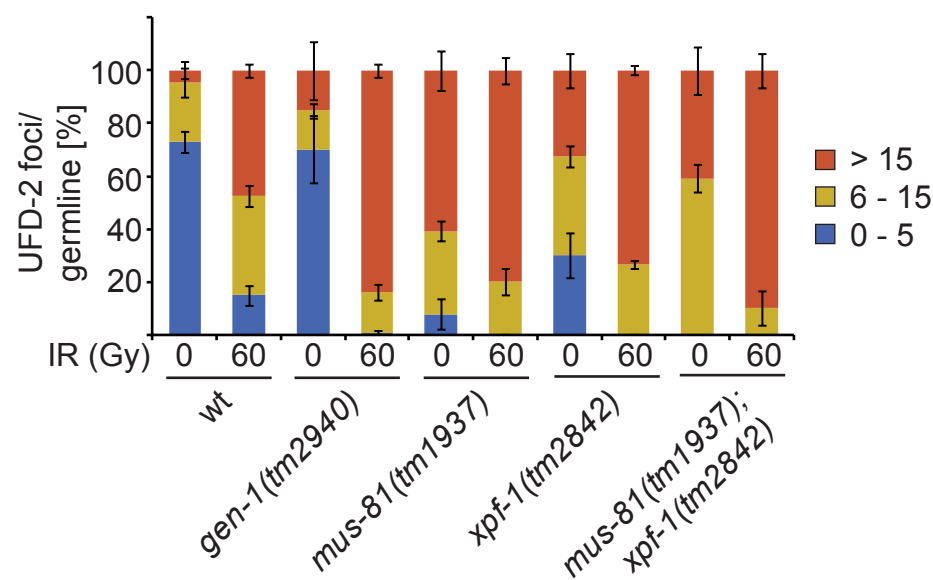
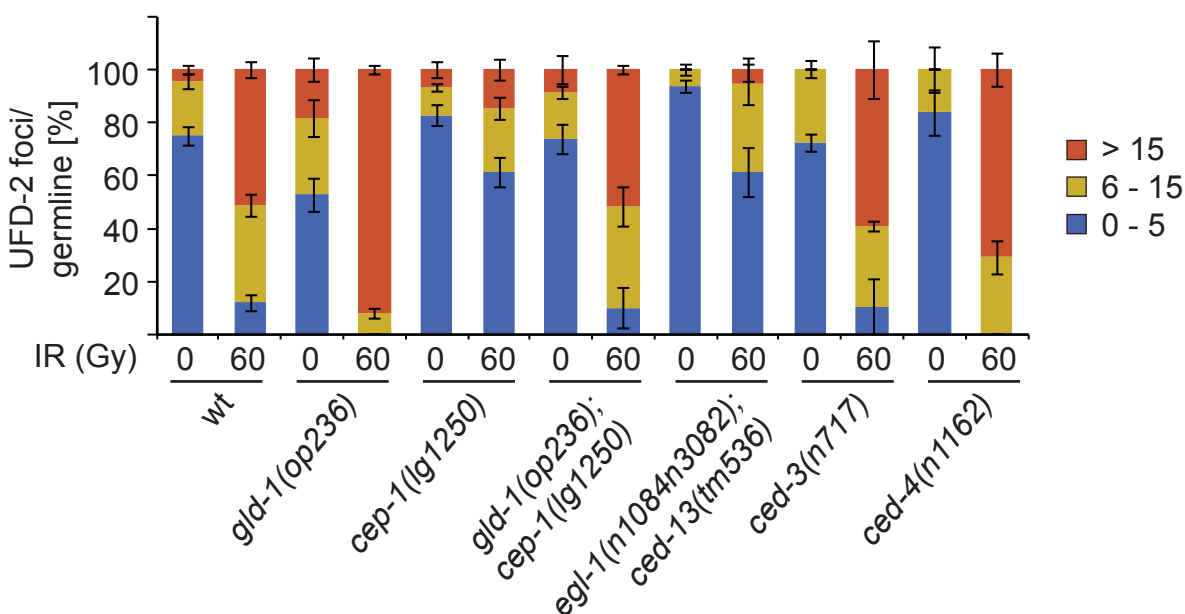
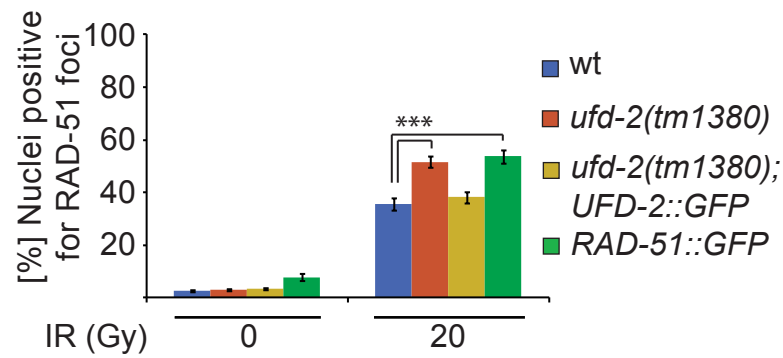
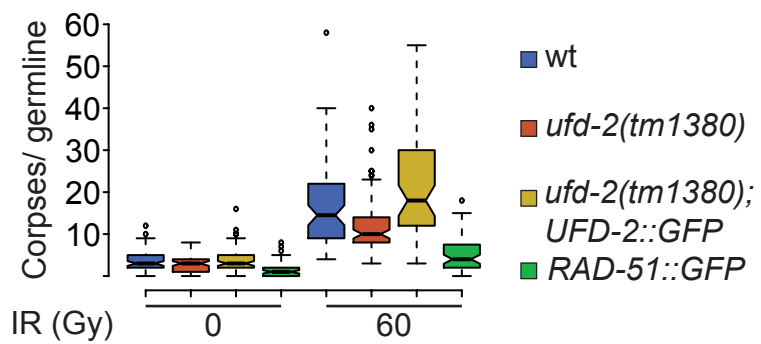
Figure 5**a****b****c****d**

Figure 6

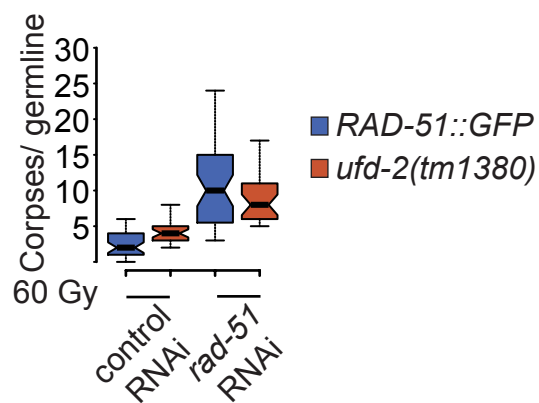
a



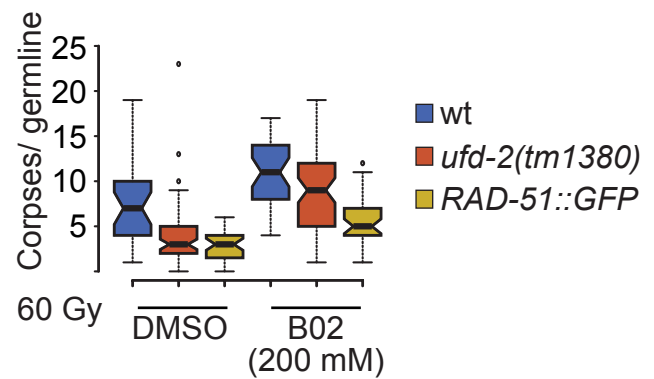
b



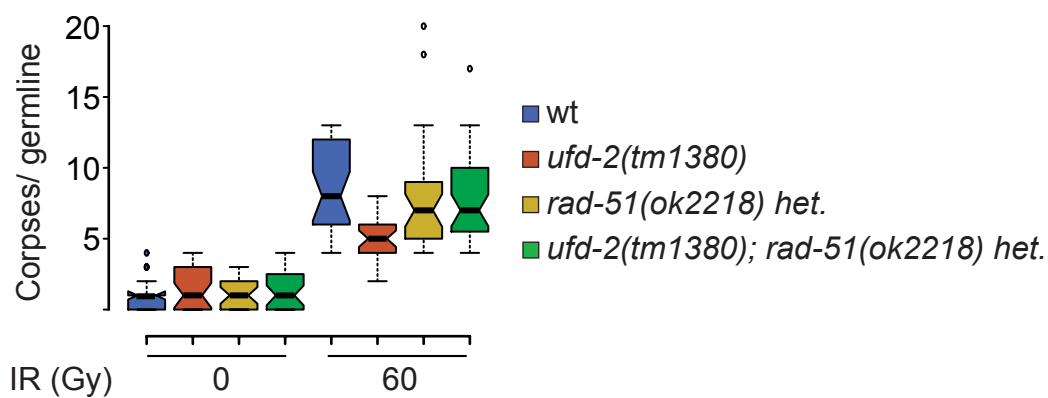
c



d



e



f

